Q. J. R. Meteorol. Soc. (2001), **122**, pp. 1–999

Ice nucleation characteristics of an isolated wave cloud

By R. J. COTTON[1]* and P. R. FIELD[1]
[1] *Meteorological Office, UK*

(Received 1 January 2001; revised 31 December 2001)

SUMMARY

This paper reports on a series of simulations of a single isolated gravity wave cloud measured during the INTACC (INteraction of Aerosol and Cold Clouds) campaign. Using a parcel model with explicit liquid and ice phase microphysics, a number of different heterogeneous nucleation modes have been tested. It has been impossible for the model to reproduce, using any of the usual nucleation modes, both the observed peak ice number concentration and ice water content while not affecting the liquid water part of the cloud. The key to simulating both of these simultaneously appears to lie in the ice nucleation occurring at a critical time during evaporation of the liquid droplets in the downdraught of the lee wave.

KEYWORDS: Ice nucleation Wave cloud Parcel model

1. INTRODUCTION

The radiative properties of ice clouds depends on their microphysical properties, such as ice water content, size spectra and crystal habit. The primary ice nucleation determines the ice production rate and size spectra, so an understanding of ice nucleation is necessary if ice clouds are to be modelled correctly. The study of ice nucleation in cirrus is hampered by the difficulty in measuring the environmental conditions and an uncertainty in the age of the ice crystals sampled. Orographic lenticular wave clouds however provide a simpler dynamical and microphysical environment.

In cold clouds, with temperatures below -35℃, the dominant ice nucleation mode is homogeneous freezing of the supercooled water droplets with the nucleation rate increasing very rapidly for colder temperatures. Nucleation rates obtained from laboratory measurements, field studies, and theoretical work all agree well (Sassen and Dodd 1988; Heymsfield and Miloshevich 1993; Pruppacher 1995). For example, Heymsfield and Miloshevich used a numerical model to show that the observed properties of a cold lenticular cloud were consistent with homogeneous freezing of solution droplets.

At temperatures warmer than -30℃, homogeneous freezing is negligible and ice nucleation must take place heterogeneously. Heterogeneous ice nucleation uses ice forming nuclei (IN) which are a special subset of atmospheric aerosols. Several heterogeneous nucleation modes are recognised:

- Deposition nucleation where water vapour is absorbed directly onto the surface of the IN where it is transformed into ice.
- Above water saturation condensation-freezing where a film of liquid is first formed on the surface of the IN and then the condensate freezes.
- Contact-freezing where the IN initiates freezing at the moment of its contact with a supercooled water drop.
- Immersion freezing nucleation where freezing of droplets is induced by IN located within the droplets themselves.

A more uncertain ice nucleation mode involves the aerosol particles resulting from evaporation of cloud droplets (Khain *et al.* 2000). During evaporation of charged droplets the

* Corresponding author: Cloud Physics Research, Met Office, Building Y46, DERA, Farnborough, Hampshire, GU14 0LX, UK. e-mail: richard.cotton@metoffice.com

charge is accumulated on the surface of the aerosol and these 'evaporation nuclei' are thought to be effective ice-forming nuclei (Beard 1992; Rosinski and Morgan 1991). If the environment also contains incompletely evaporated supercooled droplets, electroscavenging of the charged evaporation nuclei can significantly enhance the contact-freezing rate (Tinsley *et al.* 2000).

Despite many field studies and laboratory experiments, there are still uncertainties in IN concentrations and in the nucleation modes that occur in clouds. Cold wave clouds were sampled during the Subsonic Aircraft: Contrail and Cloud Effects Special Study (SUCCESS). Modelling by Jensen *et al.* (1998) of two wave cloud cases (at -37℃ and -62℃) show that deposition IN concentrations were less than 0.5 cm^{-3}. Rogers *et al.* (1998) show that deposition or condensation-freezing IN concentrations measured during SUCCESS using a continuous flow chamber were between 0.001 and 0.1 cm^{-3}. Cooper and Vali (1981) observed mountain cap clouds over -15℃ to -20℃ and concluded that the ice formed after droplet formation and that contact nucleation best fits the data. Demott (1990) performed laboratory studies on soot particles using a continuous slow expansion cloud chamber and suggested that immersion freezing is a dominant mode for ice production at temperatures warmer than -34℃.

In this paper we will report on a model-observation comparison of a single stationary isolated gravity wave cloud. This cloud was measured during flight A722 of the INTACC campaign in October 1999, by the Met. Office C-130 aircraft (see Field 2001 for details on measurements made throughout INTACC). This cloud had significant liquid water and ice at all heights with the temperature varying from -18℃ at cloud base to -32℃ at cloud top. Heterogeneous nucleation was therefore expected to be dominant. A detailed microphysical and dynamical model was used to accurately simulate the observed wave cloud with the primary aim of determining the characteristics of the ice nucleation that is occurring and determine which, if any, of the current heterogeneous nucleation schemes are dominant.

2. Instrumentation

The C-130 aircraft carried standard instrumentation which included: wind vanes, inertial navigation unit and GPS to measure vertical and horizontal winds, Rosemount probes (de-iced platinum resistance thermometer), a General Eastern cooled mirror device to measure frost point, a Lyman-α hygrometer to measure total water content, a Johnson-Williams liquid water hot wire probe, a PMS (Particle Measuring Systems) 2D-C probe to measure cloud particle concentration, and a PMS PCASP (passive cavity aerosol spectrometer probe) and a CN (condensation nucleus) counter to measure aerosol concentrations.

Various new instruments were also carried:

- A laser scattering device, SID (small ice detector). This counts and sizes spherical particles to 2μm and counts non-spherical particles. Photodetectors arranged azimuthally at a forward scattering angle give an asphericity value which indicates the dominant water phase in the cloud. A comparison with different probes, carried out in Field 2001, estimates the error on the concentration to be at most a possible overestimate by a factor of 3.
- A Nevzorov bulk water probe. Liquid water is measured by a hot wire probe where drops evaporating from the wire surface cause changes in electrical resistance. In totally glaciated conditions, the probe responds to small ice crystals which give a false liquid water content typically 20% of the total water (Korolev *et al.* 1998). The error in mass

is around 15%. Total condensed water is measured by hot wire cup which collects drops and ice crystals with an error in mass of 20%.

- A counter-flow virtual impactor (CVI) probe. Counter-flow of dry air enables only particles with mass greater than that of a 3.5μm radius droplet to enter the probe. Inside the probe the particles are evaporated and residual aerosols measured. In fully glaciated cloud, the residual aerosol concentration should therefor correspond to the ice crystal concentration.
- A cloudscope, which is essentially a video camera which views cloud particles impacting on a 0.2mm^2 window. The cloudscope can provide a visual indication of the phase of particles larger than 10μm radius.
- A continuous flow diffusion chamber IN counter. This detects deposition and immersion freezing nuclei. Ambient aerosols are subjected to ice supersaturation for several seconds. The humidity is then reduced to below water saturation to remove any liquid drops, and any remaining ice crystals give the IN concentration.

3. Wave cloud observations

The isolated wave cloud was sampled by aircraft runs at different heights. Each run was straight, level and parallel to the wind. Fig. 1 shows observations from various aircraft probes during some of these runs. No cloud particles are observed until water saturation is reached, when there is a rapid increase in cloud droplet concentration. During the water saturation region, the SID particle concentration remains constant at 200 cm^{-3}. The Nevzorov and JW water contents also increase at water saturation, reaching a maximum near the updraught-downdraught boundary. During the downdraught, near the end of the water saturation region the dominant phase of the cloud changes from liquid to ice. At this transition, several changes are observed:

- The environment becomes water subsaturated, but is still ice supersaturated.
- The SID cloud particle concentration falls rapidly to 10 cm^{-3}.
- The Nevzorov total and liquid water contents both fall and diverge.
- The average SID asphericity shows a step increase from low values typical of spherical haze particles, to high values typical of aspherical pristine ice crystals.
- On the runs where the aircraft entered the cloud from the downwind end, the cloudscope observations changed from some ice crystals to many small droplets.

Some large particles are however observed by the 2D-C probe before this phase transition, so a few ice crystals must have been initiated during the liquid water region. During the ice phase region, the SID concentration agrees with the CVI residual aerosol concentration. Disagreement during the liquid phase is because many of the supercooled haze particles are below the CVI lower size threshold. Runs just above the cloud top encountered high ice supersaturation (the environment was just below water saturation), but no cloud particles were observed. The IN counter was operated just below water saturation, and indicated that the deposition nuclei concentration upwind of the cloud was less than 0.01 cm^{-3}.

4. Wave cloud simulation

A model has been developed which simulates the microphysical and dynamical aspects of wave clouds. The cloud simulation consists of repeatedly running a parcel model

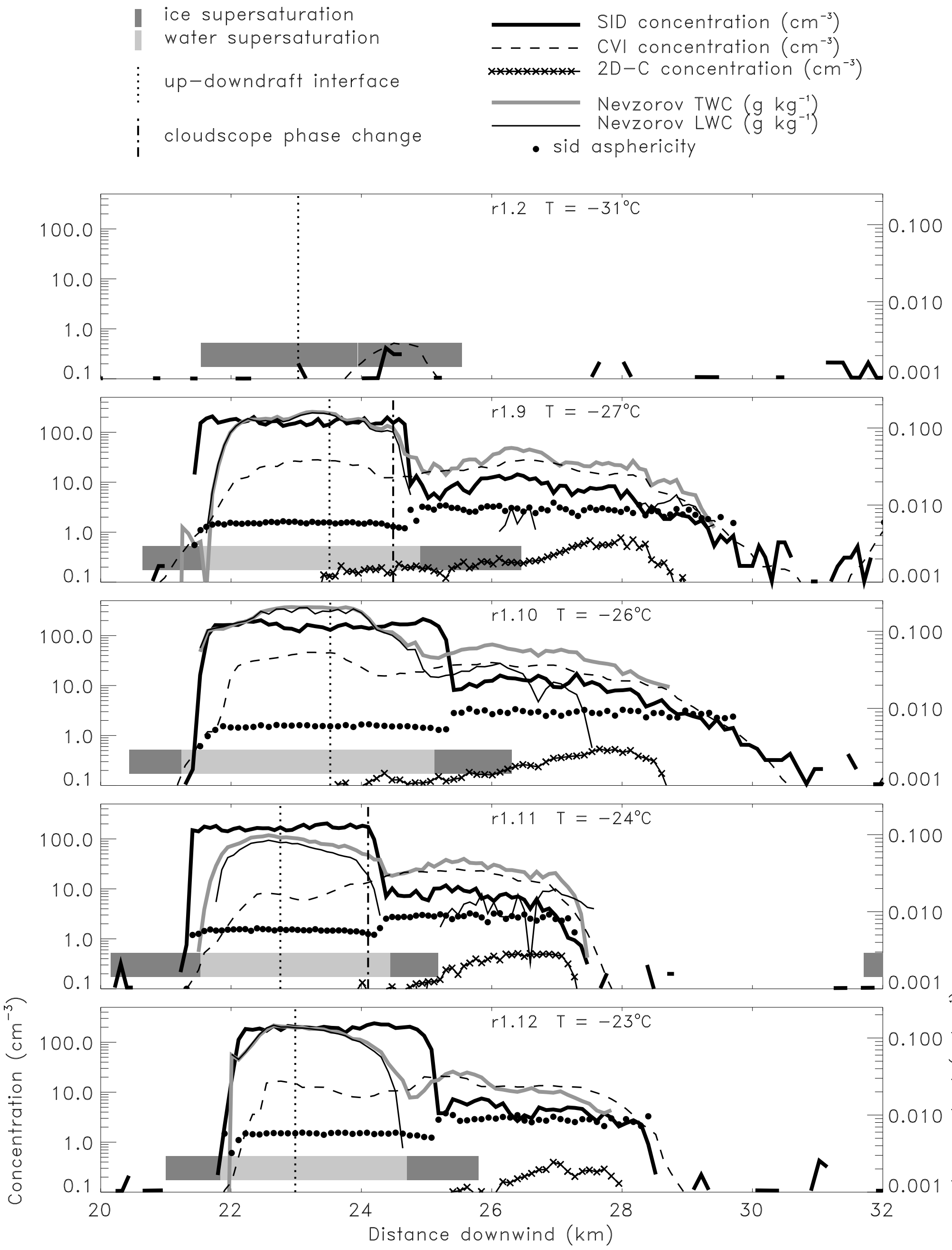

Figure 1. Five of the 14 runs through the wave cloud. The wind is blowing from left to right at 15–20 ms^{-1}. The top run was just above the cloud top. The horizontal bar shows when the air is above ice saturation (dark grey), or above water saturation (light grey). The vertical dotted line is the updraught-downdraught boundary. The vertical dot-dash line is when the cloudscope shows the dominant phase changing from ice to water.

with each parcel starting at a different height and following a different trajectory. Upwind temperature and humidity profiles define the parcel model initial temperature and water vapour mixing ratio, and measured horizontal and vertical winds define the trajectories. All parcel model runs use the same dry CCN distribution derived from the measured aerosol distribution. Fig. 2 shows some of the parcel trajectories that are used to simulate the wave cloud.

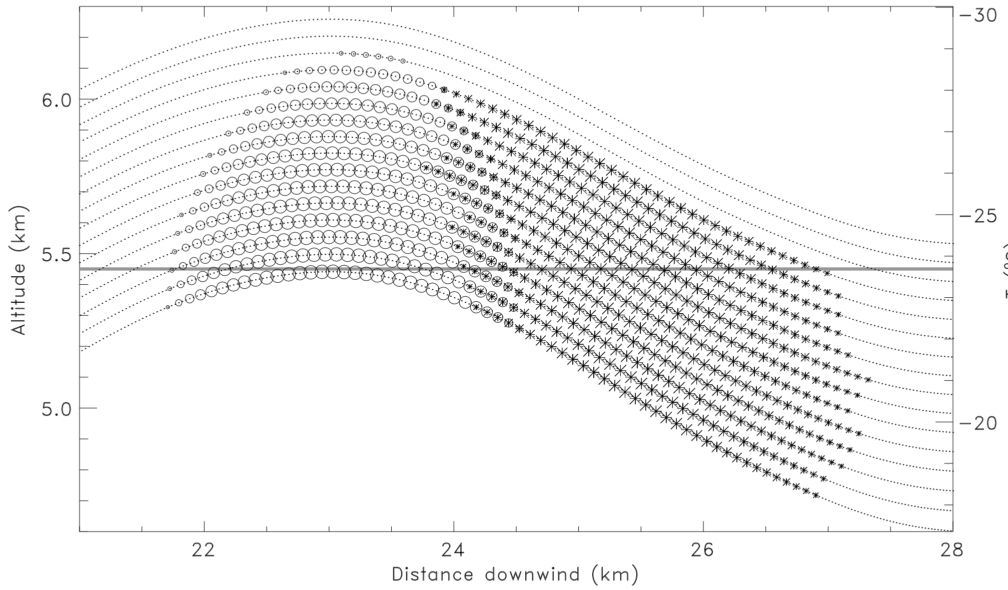

Figure 2. A wave cloud simulation of the aircraft run at the altitude marked by the grey line. Parcel trajectories are shown by the dotted lines (only every 5th trajectory is shown). Circles are drawn when there is significant liquid water, stars when there is significant ice. The size of the symbol represent the amount of water mass. There is an upwind liquid water region, a narrow mixed phase region, and an ice tail in the downdraft region. The right ordinate is the initial upstream environmental temperature, and not the parcel temperature in the cloud.

(*a*) *Parcel model description*

The parcel model is an extension of that described in Spice (1999), and was used in the GEWEX cloud systems study WG2 cirrus parcel model comparison project (see Lin R-F 2001), in which the homogeneous freezing studies all agree closely.

The model considers an adiabatic parcel of air containing a conserved mass of water. An updraft profile describes rising and falling of the parcel. At the start of the model run the dry CCN are deliquesced to the equilibrium haze droplet radii calculated using a Newton-Raphson iteration on the Kohler equation. It is assumed that the CCN have been pre-deliquesced by exposure to high ambient relative humidity. The CCN are either H_2SO_4 or $(NH_4)SO_4$, with a Van't Hoff factor of 3.

During the model run, haze and activated cloud droplets share the same bins. The bin radii are explicitly varied in time using the droplet diffusional growth rate equation (Pruppacher and Klett, 1997),

$$r\frac{dr}{dt} = \frac{1}{[F_k + F_d]}\left(\sigma_w - \frac{A_c}{r} + \frac{A_s\, r_{ccn}^3}{r^3 - r_{ccn}^3}\right) \qquad (1)$$

where σ_w is the water supersaturation, r the droplet radius and r_{ccn} the radius of the dry CCN. The terms involving A_c and A_s relate to curvature and solution effects on the drop's equilibrium vapour pressure. F_d and F_k are thermodynamic terms associated with heat conduction and vapour diffusion. F_D and F_K contain kinetic correction functions as defined by Fukuta and Walter (1970) to characterise the molecular transfer of heat and vapour. The droplet condensation coefficient α_c (0.05), the ice deposition coefficient α_d (0.24), and the thermal accommodation coefficient α_T (0.7) values are those used in Sassen and Dodd (1988). These correction functions tend reduce the diffusional growth and evaporation rates.

There are also a fixed number of ice particle radius bins, which are initially empty. (For these simulations there are 60 ice bins.) The ice particle bin radii are explicitly varied in time using the ice particle diffusional growth rate equation,

$$r_i \frac{dr_i}{dt} = \frac{\sigma_i (C/r_i)}{[F_k + F_d]} \tag{2}$$

where σ_i is the ice supersaturation, r_i the ice crystal radius, and C is a constant 'capacitance' used to represent the ice crystal habit (for spherical ice crystals $C = 1$). Ice particles may develop in these bins as a result of primary nucleation processes, either by the homogeneous freezing of supercooled water droplets or by various heterogeneous freezing processes. Ice crystals initiated by vapour deposition onto an IN are placed into the smallest 0.1μm radius bin, while droplets that freeze, because of the different ice and droplet diffusional growth rates, are partitioned between two ice particle bins so as to conserve both mass and number concentrations.

During the model run the ice particles are periodically rebinned to avoid the accumulation of large ice bins. The new bin radii are distributed logarithmically from 0.1μm to the maximum crystal size. The coupled set of differential equations involving temperature, humidity, droplet and ice bin radii and concentrations, are solved using a predictor-corrector integration scheme with a time step of $\Delta t = 0.01$s.

(*b*) *Ice particle nucleation schemes*

The homogeneous freezing rate per unit volume of water, J (cm^{3}s^{-1}), is calculated by a fit to Jeffery's (1997) formulation,

$$\begin{aligned}
T_e < -65: &\quad \log(J) = 25.63 \\
-65 \geq T_e \geq -30: &\quad \log(J) = -243.4 - 14.75T_e - 0.307T_e^2 - 0.00287T_e^3 - 0.0000102T_e^4 \\
T_e > -30: &\quad \log(J) = -7.63 - 2.996(T_e + 30)
\end{aligned} \tag{3}$$

where T_e (℃) is the effective temperature. T_e takes into account the droplet concentration and is defined by

$$T_e = T_d + \lambda\, \delta T \tag{4}$$

where T_d (℃) is the droplet temperature (which is generally not the same as the parcel temperature), λ quantifies additional non-ideal ionic interactions between the solute and liquid water during droplet freezing, and δT quantifies the melting temperature depression in less strongly bonded impure ice particles. δT is calculated using fits to standard tabulated values (Paul Demott, personal communications). For H_2SO_4,

$$\delta T = 3.514G + 0.472G^2 + 0.0332G^3 + 0.0251G^4 \quad \text{and} \quad \lambda = 2.0 \tag{5}$$

and for $(NH_4)SO_4$,

$$\delta T = 0.0220 + 4.12G - 1.331G^2 + 0.668G^3 + 0.125G^4 + 0.0083G^5 \quad \text{and} \quad \lambda = 1.7 \tag{6}$$

where G is the droplet molality (moles of solute per kg of water). This solution effect reduces the freezing rates of aqueous solution compared to pure water, and can prevent small highly concentrated haze droplets from freezing homogeneously until they have become dilute. The droplet freezing rate (number of droplets frozen per unit volume of air per second) for each droplet bin is then,

$$\left.\frac{dN_d}{dt}\right|_{hom} = JV_dN_d \tag{7}$$

where N_d (cm^{-3}) is the concentration of droplets of volume V_d (cm^3).

The following heterogeneous ice nucleation schemes are available in the model.

The number concentration $N_{d/cf}$ (cm^{-3}) of IN that act as either deposition or condensation-freezing nuclei, is described by Meyers (1992), and

$$N_{d/cf} = F\, 10^{-3} \exp\left(-0.639 + 12.96\sigma_i\right) \tag{8}$$

where σ_i is the ice supersaturation, and F is a factor which is adjusted to arbitrarily increase $N_{d/cf}$. The ice crystal initiation rate is then,

$$\left.\frac{dN_i}{dt}\right|_{dep} = 12.96 N_{d/cf} \frac{d\sigma_i}{dt} \tag{9}$$

Ice crystals are generated once the ambient humidity is above ice saturation and for a wave cloud, this is always reached before water saturation.

Contact nucleation is incorporated using the aerosol collection rates as described in Young (1974) which include Brownian motion, thermophoretic and diffusiophoretic effects. The number concentration of available contact IN, N_c (cm^{-3}), is set to some arbitrary value rather than use the parametrisation in Young (1974). The collection rates determine at what time during the model run these events occur and reduces the N_c upper limit to the potential ice-crystal concentration. The droplet freezing rate is of the form,

$$\left.\frac{dN_d}{dt}\right|_{con} \sim N_dN_c \left(A_{br}\frac{r}{r_a^2} - (A_{th} - A_{di})r\frac{dr}{dt}\right) \tag{10}$$

where r is the droplet radius, r_a the aerosol radius. A_{br},A_{th},A_{di} positive constants related to Brownian motion, thermophoretic and diffusiophoretic forcing respectively (always $A_{di} < A_{th}$) and depend on the ambient conditions and aerosol composition. This shows that:

- A larger droplet radius increases the collection rate.
- For small aerosol radius, the Brownian motion is dominant.
- For large aerosols when the droplets are evaporating the thermophoretic effect significantly enhances the collection rate.

Immersion freezing is incorporated by using the stochastic hypothesis formulated by Bigg (1953). Freezing results from random formation of a critical size embryo, and the droplet freezing rate is,

$$\left.\frac{dN_d}{dt}\right|_{imm} = V_dN_dB \exp\left(AT_d - 1\right) \tag{11}$$

where $A = 0.66℃^{-1}$ and $B = 100\ \mathrm{m^{-3}s^{-1}}$. The immersion freezing rate increases for large droplets and for colder temperatures.

(*c*) *Model initial conditions: CCN spectrum*

The dry CCN size spectrum was derived from upwind aerosol measurements using the PCASP, CNC, and SID, shown in Fig. 3. The CCN were assumed to be hygroscopic spheres of either H_2SO_4 or $(NH_4)SO_4$, lognormally distributed with the number of aerosols per unit volume with radius r to $r + dr$ given by

$$N(r)dr = \frac{N_t}{\sqrt{2\,\pi}} \exp\left[-\frac{1}{2}\left(\frac{\ln r - \ln r_g}{\ln \sigma}\right)^2\right] d(\ln r) \tag{12}$$

The PCASP accumulation mode lognormal fit had the constraint that the total number N_t was that measured by the CNC (giving $r_g = 0.11\mu$m, $\sigma = 1.565\mu$m). The distribution was then binned with 50 logarithmically increasing bin widths to provide the model input. The lognormal distribution of the clear-air SID and PCASP coarse mode aerosols were binned to give a further 10 points for the initial CCN spectrum (where $N_t = 0.244$,$r_g = 1.1\mu$m, $\sigma = 1.657\mu$m).

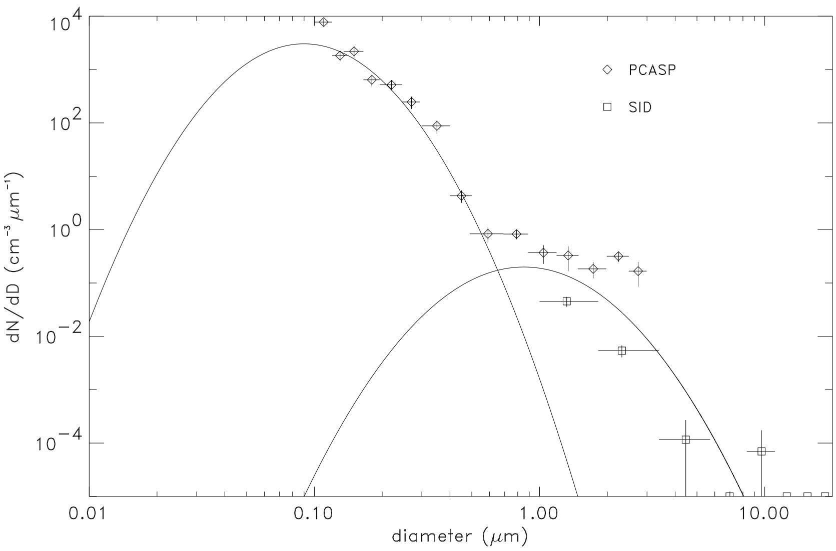

Figure 3. Dry CCN spectrum derived from upwind aerosol measurements, made in clear air using SID and PCASP. The lines are the fitted lognormal functions to the accumulation and coarse mode aerosols.

(*d*) *Model initial conditions: Temperature and water vapour mixing ratio*

Each parcel model run must be initialised with the air temperature and frost point or water vapour mixing ratio. Because each streamline starts at a different height the environmental temperature and humidity profiles, defined at the cloud simulation starting distance (around 5 km upwind of the cloud leading edge), are required.

Profiles were derived from out of cloud (both upwind and downwind) temperature and relative humidity measurements made along the run. Each measurement of temperature and total water content is moved adiabatically along a streamline to the upwind starting distance to give temperature and water vapour mixing ratio as a function of height. The resulting profiles Fig. 4(a) and Fig. 4(b) however are not very good. The aircraft kept constant altitude during each run, cutting through many parcel streamlines more than once (see Fig. 2) and Observations from the same streamline should give the similar temperature and humidities at the starting height.

The simplest way of improving the temperature and humidity profiles is to offset the vertical wind measurements. The profiles Fig. 4(c) and Fig. 4(d) were obtained by adding a constant 0.5 ms^{-1} to the vertical wind. This offset only has to be applied because of the error in vertical wind from the wind-vanes. The offset depends on the aircraft run that is being modelled and was typically 0–0.5 ms^{-1}. Usually, for wind-vane measurements where the runs are long the average vertical wind is subtracted, but here the runs are short and are in disturbed air so this is not done.

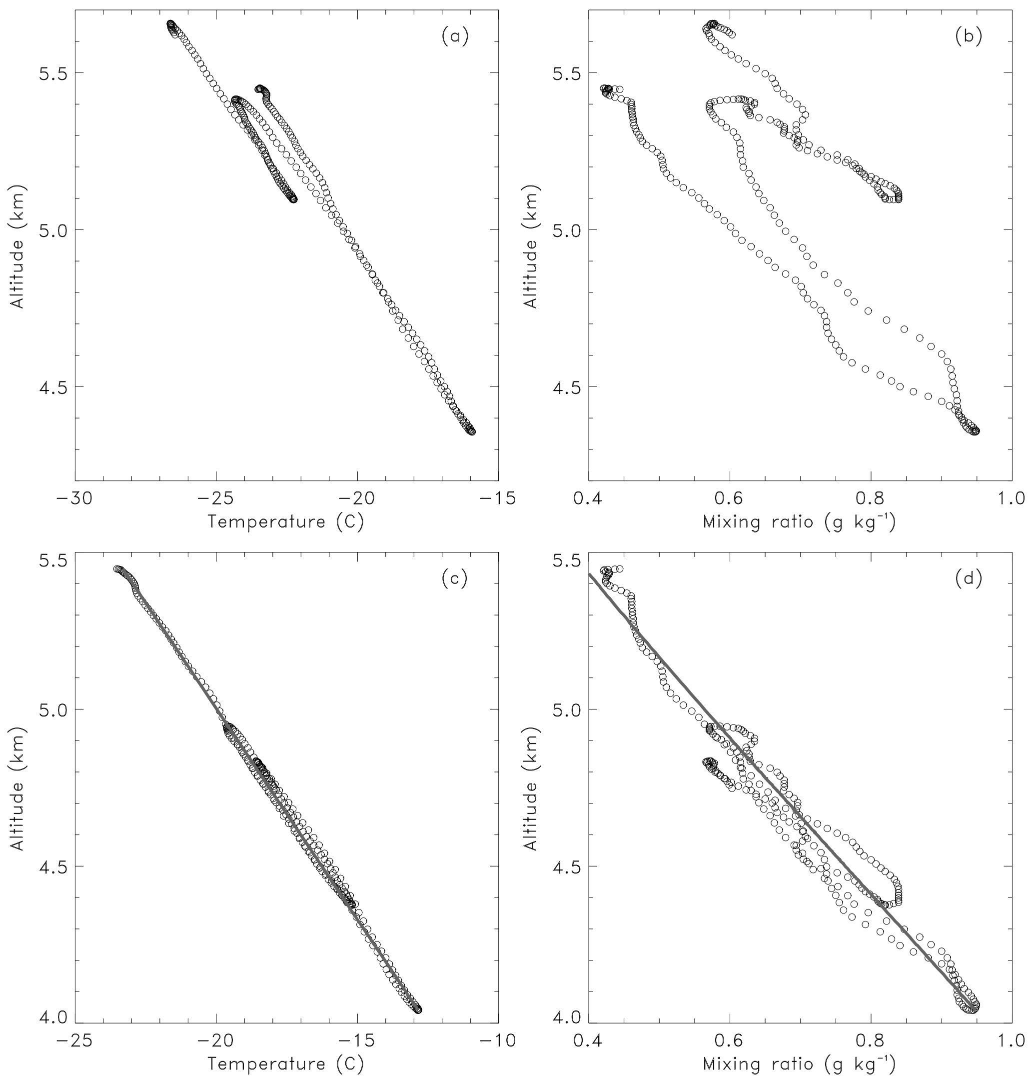

Figure 4. Temperature and humidity profiles defined at the cloud simulation start distance, derived from aircraft observations made along run r1.11. For (a) and (b) no vertical wind offset was applied (a) and (b), while for (c) and (d) the offset was 0.5 ms^{-1}. The lines are the fitted environmental lapse rate (linear fit) and the water vapour mixing ratio (polynomial fit).

A linear fit to the temperature profile gives the environmental lapse rate, and the frost point as a function of height is given by a polynomial fit to the water vapour mixing ratio profile. A horizontal wind shear must also be used because parcels have large vertical excursions. Fig. 5 shows the aircraft observations and model values of vertical wind, temperature and relative humidity along run r1.11. The environmental conditions along this run are well modelled. If the cloud simulation used a non-corrected vertical wind to determine the parcel trajectories, then the humidity would be very wrong and the detailed microphysics could not be accurately simulated.

5. Model-observation comparisons

The critical aspects that the model must get correct, are:

- Few cloud particles (above 1μm radius) until water saturation is reached.
- Significant liquid water mass (reaching 0.06–0.15g kg^{-1}).
- The dominant phase changing from liquid to ice during the downdraught.
- Ice concentrations of 10 cm^{-3}, for droplet concentrations of ≈ 200 cm^{-3}.

Simulations of a series of aircraft runs through the main part of the cloud were made. Various primary ice nucleation schemes were used with the aim of determining the ice nucleation characteristics which best fits the observed data. Fig. 6 and Fig. 7 show, for aircraft run r1.11, a series of simulations each using a different nucleation scheme. The coldest temperature reached by the parcel for this aircraft run is around -30℃, so homogeneous freezing is negligible (the droplet-environment temperature difference due to evaporation is small). The homogeneous freezing only simulation (Fig. 6(a)) does show that the liquid water cloud start and end distance, and total water content are well modelled. The discrepancy in the total water content may be partly due to the probe error when the airflow enters the inlet at different pitch angles because of the wave cloud streamlines. Even for the highest run shown in Fig. 1, which was just below cloud top, the model predicts little homogeneous freezing.

Deposition nucleation (Fig. 6(b) and Fig. 6(c)) is not expected to be the dominant mode. This is because the IN counter measured few deposition nuclei, runs immediately above cloud top encountered ice supersaturation but no ice was observed, and deposition nuclei will tend to be activated before the liquid water phase (in a wave cloud, ice supersaturated is always reached before water supersaturation). Increasing the deposition/condensation-freezing rate by using $F = 5$ (Fig. 6(b)) gives the required ice water content but there are too few ice crystals, while increasing it by using $F = 100$ (Fig. 6(c)) generates too much ice water mass from the required ice number concentration.

Contact nucleation (Fig. 7(a)) where Brownian motion dominates the collection rates (small aerosol radius) achieves the measured ice concentration. While some ice crystals are formed by collisions with haze particles, most are formed when the droplets are larger. However the ice water mass is still too high and the liquid water growth is inhibited.

Immersion freezing (Fig. 7(b)) forms ice crystals after the peak of the liquid water cloud when the droplets are large and the temperature is coldest. To get the measured ice crystal concentration the constant B is increased to 10^4 m^{-3}s^{-1} since there are large uncertainties on B which depends on the droplet solution. The ice water mass is still too high however, but the liquid water peak is well matched.

Contact nucleation (Fig. 7(c)), where the thermophoretic effect enhances the collection rates (large aerosol radius) causes ice to be formed during the rapid droplet evaporation region in the downdraught. However the collision rate is too low, so that

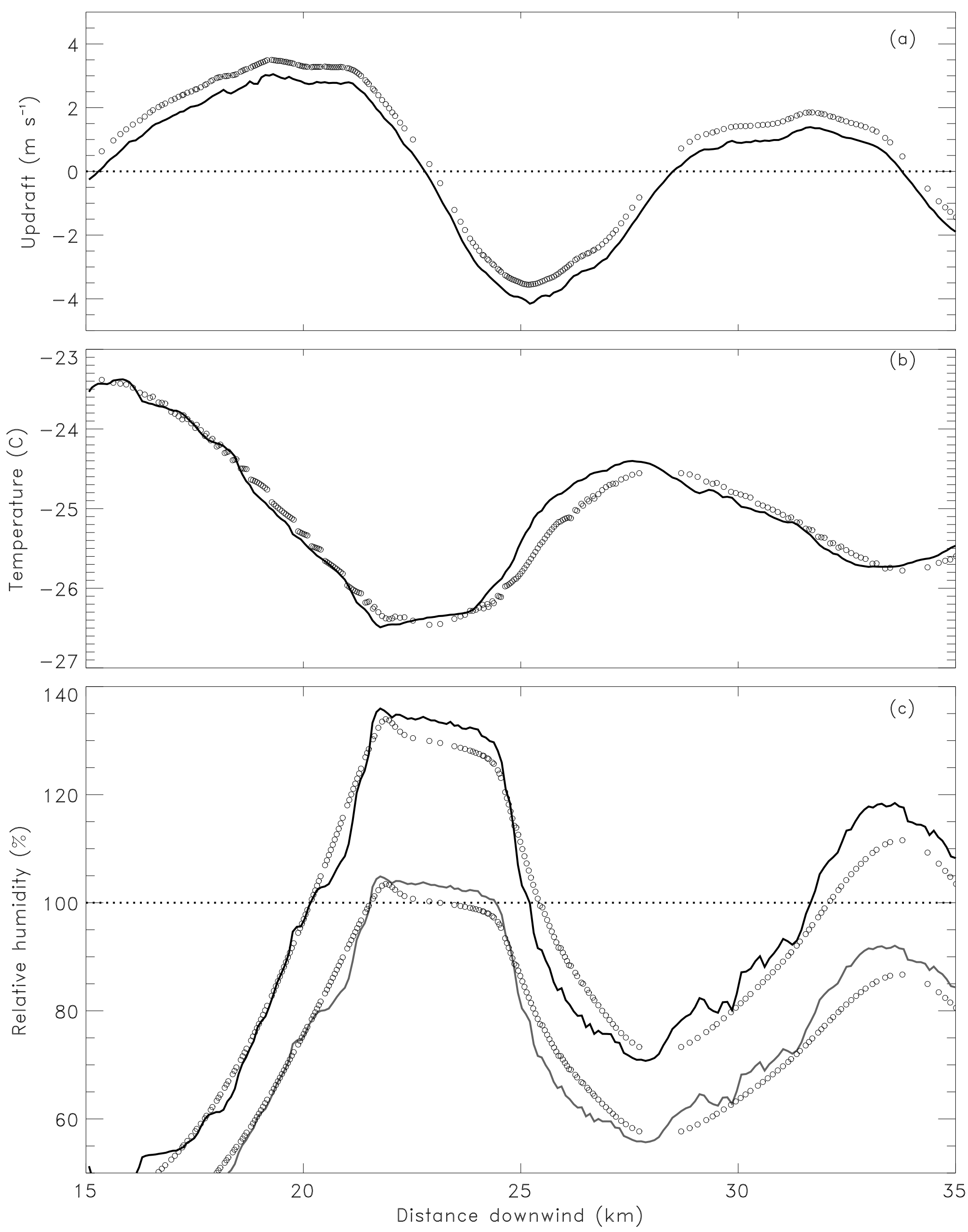

Figure 5. Thermodynamic *in-situ* observations made along run r1.11 of, (a) the vertical wind, (b) temperature, and (c) relative humidities w.r.t. water and ice. The solid lines are the aircraft observations. Each symbol is from a model streamline intersecting the aircraft altitude.

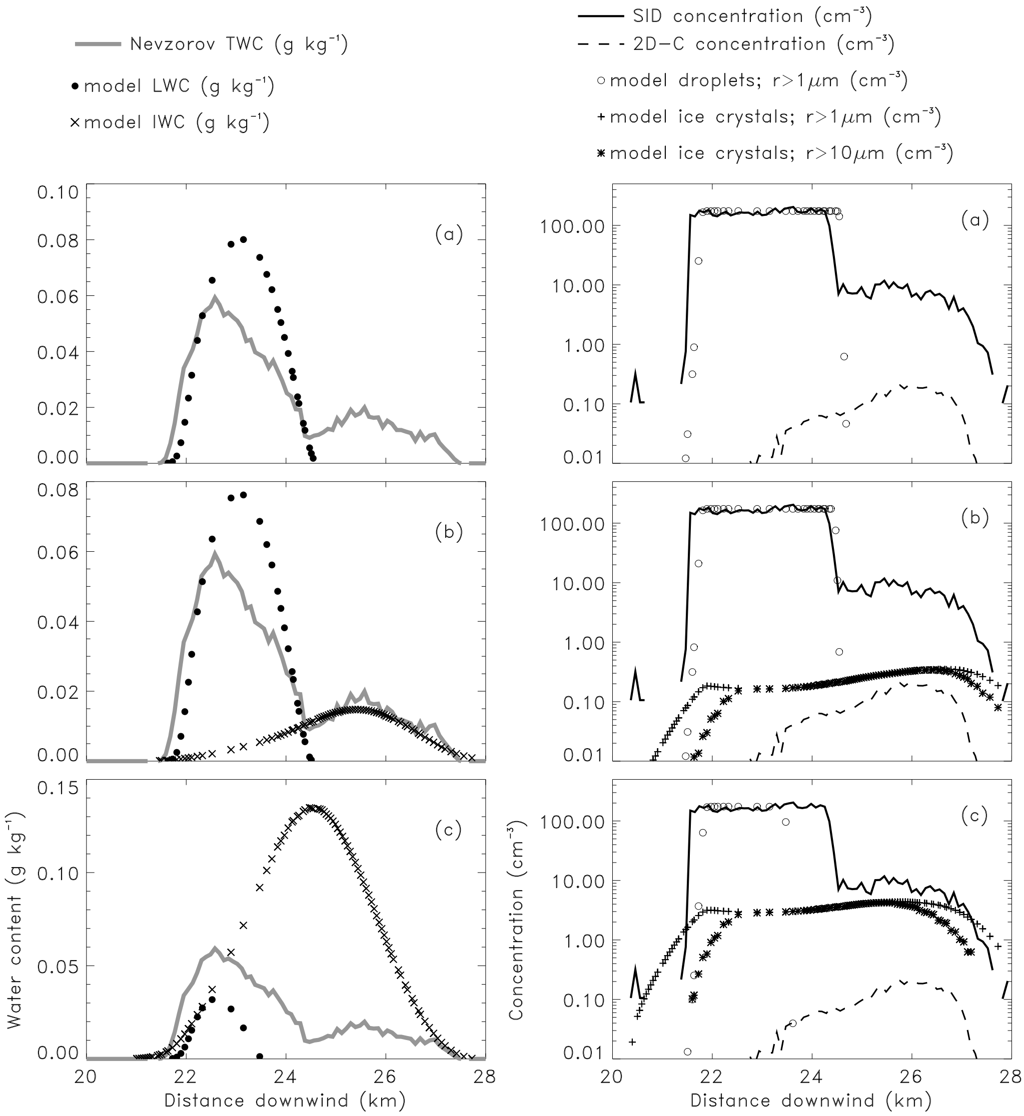

Figure 6. Aircraft run r1.11 simulations using various ice nucleation schemes; (a) homogeneous freezing of $(NH_4)SO_4$ solution droplets, (b) combined deposition and condensation-freezing where $F = 5$, and (c) where $F = 100$.

even with the maximum possible aerosol concentration, the modelled ice concentration is an order of magnitude too small.

An arbitrary 'evaporation-onset' nucleation scheme (Fig. 7(d)) can be used to show that to achieve the observed liquid and ice water mass and concentration characteristics, most ice crystals must be formed near the end of the liquid water evaporation region. Because of the very rapid increase in droplet concentration once water subsaturation is reached, a concentration threshold was used to activate the freezing of each droplet bin. Similar to homogeneous freezing, a stochastic freezing rate is defined by,

$$\left.\frac{dN_d}{dt}\right|_{evap} = V_d N_d J_e \tag{13}$$

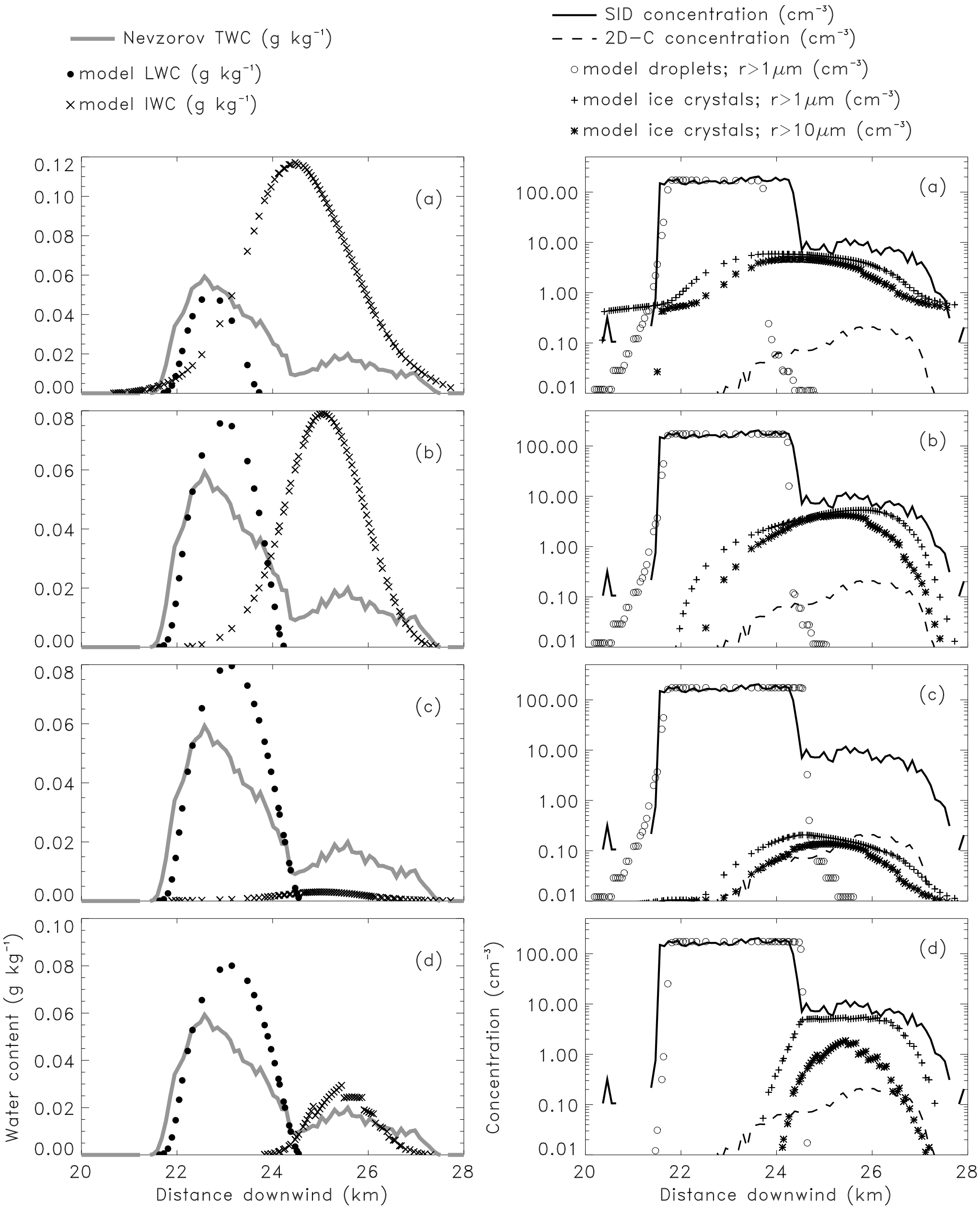

Figure 7. Aircraft run r1.11 simulations using various ice nucleation schemes; (a) contact nucleation where $r_a = 0.01\mu$m, $N_c = 400$cm^2, (b) immersion-freezing where $B = 10^4$ m^{-3}s^{-1}, (c) thermophoretically enhanced contact nucleation where $r_a = 0.1\mu$m, $N_c = 400$cm^2, and (d) evaporation-onset freezing where $J_e 2 \times 10^{14}$ m^{-3}s^{-1}.

where J_e is a constant (2×10^{14} m^{-3}s^{-1}) arbitrarily chosen to give the observed ice crystal concentration. For simplicity J_e is not defined as a function of temperature. This nucleation scheme is not describing any microphysics, and the choice of the freezing rate equation is not critical—its just a method of generating the observed ice crystal concentration at a specific time.

The tendency for ice nucleation schemes that create ice crystals later in the wave cloud to better fit the observations is shown more clearly in Fig. 8 which shows two aircraft run simulations at different heights through the cloud. The ice concentration and water contents plotted on the graph are the maximum obtained in the ice tail. Results from cloud simulations using the same ice nucleation scheme but with different 'scaling constants' lie along the same line. The position along the line is determined by:

- For deposition nucleation, the factor F which increases the number $N_{d/cf}$ of IN that are activated.
- For contact nucleation, the total number N_c of aerosol available.
- For immersion freezing, the droplet freezing activity B.
- For evaporation-onset freezing, the constant J_e.

These all have large uncertainties so the actual position along the line is not well constrained, although the depletion of liquid water puts a constraint on the upper limit.

Changing some of the constants used in the parcel model tends to move these lines further from the ice mass/concentration observation. The 'capacitance' C used in the ice crystal growth rate equation is nominally set to $C = 0.3$ to represent non-spherical ice crystals. Assuming a spherical ice crystal habit by setting $C = 1.0$, slows the ice growth and moves the deposition line further to the left. The ice crystal density is nominally set to 1.0×10^3 kg m^{-3}. Reducing the density to 0.5×10^3 kg m^{-3} also slows the ice growth and moves the deposition line further to the left. Changing the coefficients α_c, α_d and α_T used in the calculation of the kinetic correction functions F_d and F_k within reasonable limits has only a small effect.

The similar gradients might imply that these lines are a characteristic of the wave cloud environmental conditions.

6. Discussion and conclusion

The environmental conditions in wave clouds are forced by the dynamics. To accurately simulate wave cloud observations, it is therefore critical to know the wind field over the height of the cloud, in addition to good upstream temperature and humidity profiles. For wind measurements using a wind-vane system, there is an unknown constant offset on the timescales of the runs. It is important to correct the vertical wind (using a constant offset), otherwise the humidity will be simulated incorrectly when the height displacement of the parcel is estimated by integrating the vertical velocity.

Observations indicate, and modelling confirms, that for the wave cloud measured during flight A722, the presence of water droplets is a prerequisite for ice crystal generation. This agrees with the mountain cap cloud observations of Cooper and Vali (1981) who reported that droplets were generated first followed by ice.

The droplet temperatures were too warm ($T_d > -30$ ℃), even during rapid evaporation, for significant homogeneous freezing. Simulations with different heterogeneous nucleation modes can be summarised by plotting the maximum ice water content as a function of maximum ice crystal concentration. Each nucleation mode forms a line with a similar gradient, which depends on the environmental conditions. Where the IN activation occurs later in the cloud, this line moves further to the right. The wave cloud

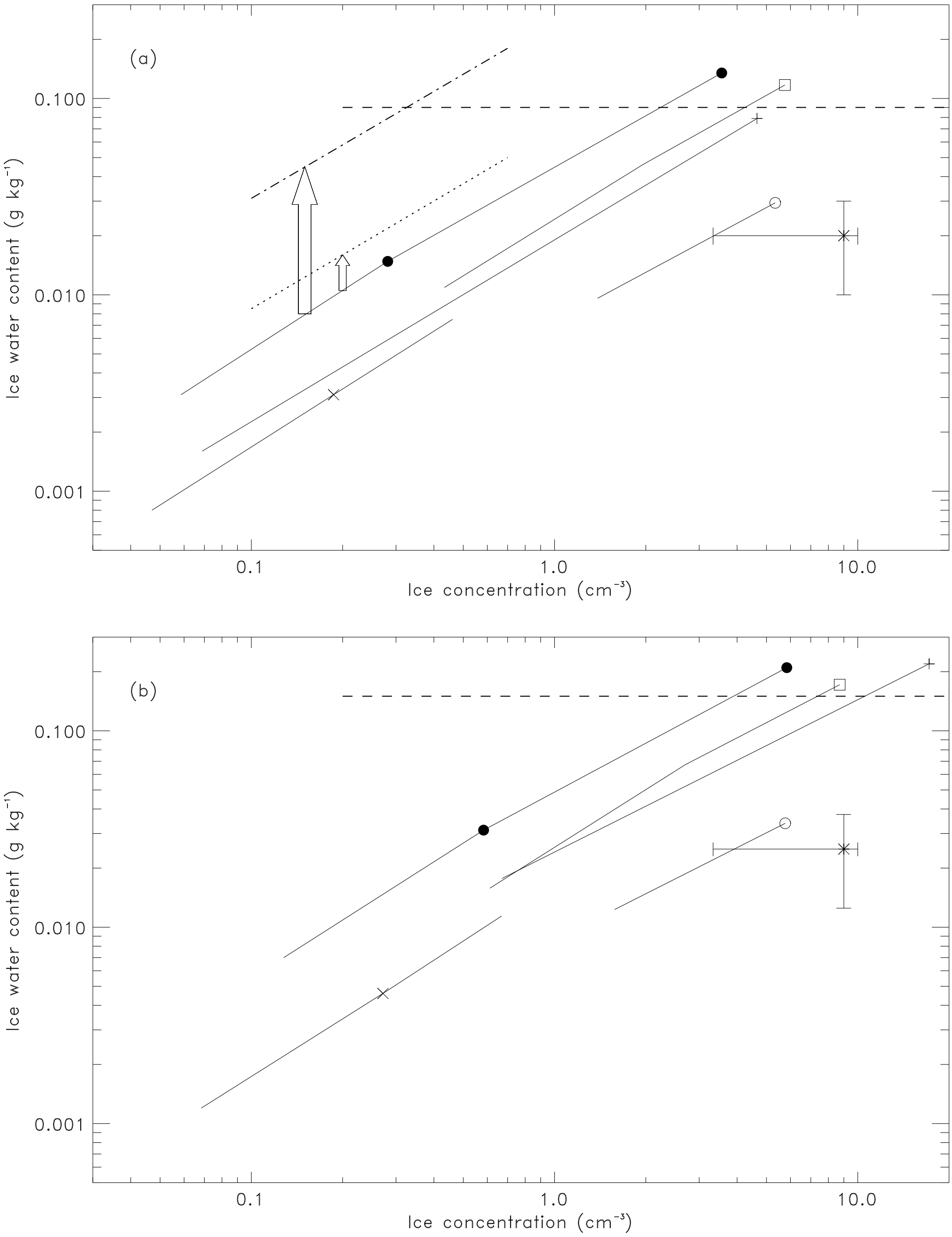

Figure 8. Simulated peak ice values for aircraft run r1.11 (a) and for run r1.9 (b). Results from each heterogeneous nucleation mode lie along a different line. The symbols are for those runs that are shown in Fig.5 and Fig.6. Deposition/condensation-freezing lie along the line with • symbols, contact nucleation where Brownian motion dominates ($r_a = 0.01\mu$m) with □ symbols, thermophorectically enhanced contact nucleation ($r_a = 0.1\mu$m) with × symbols, immersion freezing with + symbols, and evaporation-onset freezing with ○ symbols.
Reducing the ice crystal density to 0.5 kg m^{-3} moves the deposition/condensation-freezing onto the dotted line. Increasing the ice crystal capacitance to $C = 1.0$ moves the deposition/condensation-freezing onto the dot-dash line. The observed peak ice mass-concentration are the $*$ symbols with estimated 95% confidence limit error bars. Above the dashed line the ice significantly reduces the liquid water peak.

model cannot reproduce, using any of the usual heterogeneous nucleation modes, both the observed peak ice number concentration and ice water content while not affecting the liquid water part of the cloud. To simulate both of these simultaneously, the ice nucleation must occur at a critical time during the rapid evaporation of the liquid droplets in the downdraught of the lee wave.

This conclusion depends on high ice concentrations of typically 10 cm^{-3} being correct. The SID droplet concentration is well modelled, and the SID and CVI agree well in the ice phase. Additionally, during another INTACC flight where the temperature was low enough for homogeneous freezing to be dominant, the ice concentration was similar to the initial droplet concentration (see Field 2001).

The significant liquid water mass implies that the dominant heterogeneous nucleation mode that is occurring in this cloud is not deposition nucleation. Deposition IN will activate before water supersaturation is reached and many rapidly growing ice crystals will inhibit droplet growth. Both condensation-freezing or stochastic immersion freezing are also not the dominant nucleation mode. Changing the ice crystal capacitance and density from the model nominal values makes this conclusion more robust.

The best-fit to the observations is that the ice nucleation occurs at a critical time during evaporation of the liquid droplets in the downdraught. Thermophoretically enchanced contact nucleation occurs during rapid droplet evaporation but the collision rates are too low. One speculative 'evaporation-onset' nucleation mode that may give the observed ice crystal concentration is contact nucleation enhanced by electroscavenging of charged aerosols from evaporated cloud droplets. In the downdraught the larger droplets are last to evaporate, and collision rates increase with droplet size. Additionally the downdraught timescales are comparable to the charge decay times for droplets in the atmosphere. However, because the actual charge on the droplets is unknown (indeed so too is the mechanism to initially charge the droplets) the electroscavenging collision rate cannot be calculated.

7. Acknowledgements

Financial support for this work was given by the EU under the contract ENV4-CT97-0549. Support is acknowledged from the Swedish Air Force Jamtland Air Wing (F4) in Ostersund, Sweden, and from the Swedish Meteorological service. The Royal Air Force aircrew and ground crew of the Met Office C-130 aircraft are also thanked.

References

Beard, K. V. 1992 Ice initiation in warm-base convective clouds: an assessment of microphysical mechanisms. *Atmos. Res.*, **28,** 125–152

Bigg, E. K. 1953 The formation of atmospheric ice crystals by the freezing of droplets. *Q. J. R. Meteorol. Soc.*, **79,** 510–519

Cooper, W. A. and Vali, G. 1981 The origin of ice in mountain cap clouds. *J. Atmos. Sci.*, **38**(6), 1244–1259

DeMott, P. J. 1990 An exploratory study of ice nucleation by soot aerosols. *J. Appl. Meteorol.*, **29,** 1072–1079

Field, P. R., Cotton, R. C., Noone, K., Glantz, P., Keye, P. H., Hirst, E., Greenaway, R. S., Jost, C., Grabriel, R., Reiner, T., Andreae, M., Saunders, C. P. R., Archer, A., Choularton, T., Smith, M., Brooks, B., Hoell, C. Bandy, B., Johnson, D. and Heymsfield, A. 2001 Ice nucleation in orographic wave clouds: Measurements made during INTACC. *Q. J. R. Meteorol. Soc.*, **127,** 1–20

Fukuta, N. and Walter, L. A. 1970 Kinetics of hydrometeor growth from a vapor-spherical model. *J. Atmos. Sci.*, **27,** 1160–1172

Heymsfield, A. J., Miloshevich, L. M. 1993 Homogeneous ice nucleation and supercooled liquid water in orographic wave clouds. *J. Atmos. Sci.*, **50**(15), 2335–2353

Jeffery, C. A. and Austin, P. H. 1997 Homogeneous nucleation of supercooled water: Results from a new equation of state. *J. Geophys. Res.*, **102**(D21), 25269–25279

Jensen, E. J., Toon, O. B., Tabazadeh, A., Sachse, G. W., Andersen, B. E., Chan, K. R., Twohy, C. W., Gandrud, B., Aulenbach, S. M., Heymsfield, A., Hallet, J. and Gary, B. 1998 Ice nucleation processes in upper tropospheric wave clouds observed during SUCCESS. *Geophys. Res. Lett.*, **25**(9), 1363–1366

Khain, A., Ovtchinnikov, M., Pinsky, M., Pokrovsky, A. and Krugliak, H. 2000 Notes on the state-of-the-art numerical modeling of cloud microphysics. *Atmos. Res.*, **55,** 159–224

Korolev, A. V., Strapp, J. W., Isaac, G. W. and Nevzorov, A. N. 1998 The Nevzorov airborne hot-wire LWC-TWC probe: Principle of operation and performance statistics. *J. Atmos. Oceanic Technol.*, **15,** 1495–1510

Meyers, M. P., DeMott, P. J. and Cotton, W. R. 1992 New primary ice-nucleation parameterizations in an explicit cloud model. *J. Appl. Meteorol.*, **31,** 708–721

Pruppacher, H. R. 1995 A new look at homogeneous ice nucleation in supercooled water drops. *J. Atmos. Sci.*, **52,** 1924–1933

Pruppacher, H. R. and Klett, J. D. 1997 *Microphysics of clouds and precipitation. 2nd edn.* Oxford Press, 919 p

Rogers, D. C., Demott, P. J. Kreidenweis, S. M. and Chen, Y. 1998 Measurements of ice nucleating aerosols during SUCCESS. *Geophys. Res. Lett.*, **25**(0), 1383–1386

Rosinski, J., Morgan, G. 1991 Cloud condensation nuclei as a source of ice-forming nuclei in clouds. *J. Aerosol Sci.*, **22,** 123–133

Sassen, K., Dodd, G. C. 1988 Homogeneous nucleation rate for highly supercooled cirrus cloud droplets. *J. Atmos. Sci.*, **45,** 1357–1369

Spice, A., Johnson, D. W., Darlison, A. G. and Saunders, C. P. R. 1999 Primary ice nucleation in orographic cirrus clouds: A numerical simulation of the microphysics. *Q. J. R. Meteorol. Soc.*, **125,** 1637–1667

Tinsley, B. A., Rohrbaugh, R. P., Hei, M. and Beard, K. V. 2000 Effects of image charges on the scavenging of aerosol particles by cloud droplets and on droplet charging and possible ice nucleation schemes. *J. Atmos. Sci.*, **57,** 2118–2134

Young, K. C. 1974 The role of contact nucleation in ice phase initiation in clouds. *J. Atmos. Sci.*, **31,** 768–776